HHS Public Access

Author manuscript

J Biomed Mater Res B Appl Biomater. Author manuscript; available in PMC 2022 March 01.

Published in final edited form as:

J Biomed Mater Res B Appl Biomater. 2021 March ; 109(3): 394–400. doi:10.1002/jbm.b.34707.

Preclinical Assessment of Clinically Streamlined, 3D-Printed, Biocompatible Single- and Two-Stage Tissue Scaffolds for Ear Reconstruction

Julia R. Brennan, MD[a,#], **Ashley Cornett**[b,c,#], **Brian Chang, MD MS**[d], **Sarah J. Crotts, MS**[e], **Zahra Nourmohammadi, PhD**[a], **Isabelle Lombaert, PhD**[b,c], **Scott J. Hollister, PhD**[e], **David A Zopf, MD, MS**[a,f]

[a]Department of Otolaryngology–Head and Neck Surgery, University of Michigan, 1540 E Hospital Dr., Ann Arbor, MI, 48109, USA

[b]Department of Biologic and Materials Sciences & Prosthodontics, School of Dentistry, University of Michigan, 1011 N University, Ann Arbor, MI 48109

[c]Biointerfaces Institute, University of Michigan, 2800 Plymouth Rd, Ann Arbor, MI 48109

[d]Department of Pediatrics, UCLA Mattel Children's Hospital, 757 Westwood Plaza, Los Angeles, CA 90095, USA

[e]Center for 3D Medical Fabrication, Coulter Department of Biomedical Engineering, Georgia Institute of Technology, 313 First Drive, Atlanta, GA, 30332, USA

[f]Department of Biomedical Engineering, Michigan Engineering, Ann & Robert H. Lurie Biomedical Engineering Building, 1101 Beal Ave., Ann Arbor, MI 48109, USA

Abstract

Auricular reconstruction is a technically demanding procedure requiring significant surgical expertise, as the current gold standard involves hand carving of the costal cartilage into an auricular framework and re-implantation of the tissue. 3D-printing presents a powerful tool that can reduce technical demands associated with the procedure. Our group compared clinical, radiological, histological, and biomechanical outcomes in single- and two-stage 3D printed auricular tissue scaffolds in an athymic rodent model.

Briefly, an external anatomic envelope of a human auricle was created using DICOM computed tomography (CT) images and modified in design to create a two-stage, lock-in-key base and elevating platform. Single- and two-stage scaffolds were 3D printed by laser sintering poly-L-caprolactone (PCL) then implanted subcutaneously in five athymic rats each. Rats were monitored for ulcer formation, site infection, and scaffold distortion weekly, and scaffolds were explanted at

Corresponding author prior to final publication: Brian Chang. **Corresponding author contact information for final publication**: David A. Zopf, MD, Department of Otolaryngology, University of Michigan, 1540 E. Hospital Dr., CW 5-702, SPC 4241, Ann Arbor, MI 48109, Tel.: + 1 734-936-9816, davidzop@umich.edu.
[#]Shared first authors

This manuscript was presented as a podium presentation at the Annual Academy of Otolaryngology – Head and Neck Surgery Meeting in New Orleans, LA, September 18, 2019.

eight weeks with analysis using microCT and histologic staining. Nonlinear finite element analysis was performed to determine areas of high strain in relation to ulcer formation.

Scaffolds demonstrated precise anatomic appearance and maintenance of integrity of both anterior and posterior auricular surfaces and scaffold projection, with no statistically significant differences in complications noted between the single- versus two-staged implantation. While minor superficial ulcers occurred most commonly at the lateral and superior helix coincident with finite element predictions of high skin strains, evidence of robust tissue ingrowth and angiogenesis was visible grossly and histologically. This promising preclinical small animal model supports future initiatives for making clinically viable options for an ear tissue scaffold.

Keywords

3D-printing; auricular reconstruction; bioscaffolds; nonlinear finite element analysis

Introduction

Auricular reconstruction provides a solution for many children in the US born with congenital anomalies including microtia and anotia. Children with facial deformities are at risk of social and psychological stress and decreased quality of life.[1] Failure to reconstruct the ear can have significant sequelae on the child's psychosocial development and can result in functional impairment for eyeglass wear or hearing aids.

Auricular reconstruction presents a uniquely challenging endeavor in part due to the complex 3-dimensional (3D) geometry of the auricle. The current standard of care for ear reconstruction includes the staged use of autologous rib cartilage grafting which creates a support for overlying soft tissue.[2] This technique requires a high degree of surgical and artistic skill and its adoptability is limited to a select number of experienced surgeons. Moreover, the operation requires substantial rib cartilage resection and can delay the initiation of ear reconstruction until the child is of adequate age.[3] Additionally, there are significant disadvantages to the method including the associated donor site morbidity, lengthy operative time, and risks including pneumothorax and infection.[4] At least 2 staged surgeries are required, gradually introducing cartilage under the skin, limiting strain to the overlying skin that would be generated if all cartilage were implanted at once.

Alternatives to this method include alloplastic, high density porous polyethylene implants or the use of an ear prosthesis. These too are limited by significant disadvantages including risks extrusion – potentially from the high volume of implant material placed at once and resultant overlying skin strain - infection, fracture, operative time, and cost.[5] In addition, these implants are not patient-specific and thus do not always reflect the anatomy of the patient's contralateral ear. Alternative studies have looked at using a mold to tissue-engineer a human-sized auricle of normal anatomic definition in a large animal model. Further work is required in this area before it might reach human trials including determining the feasibility of re-implanting the structure and maintaining the delicate shape and size.[6]

In prior efforts, our research team has demonstrated the utility of using additive manufacturing, patient-specific imaging, and image-based design to replicate complex craniofacial structures through high-fidelity tissue bioscaffolds.[7–10] The techniques utilized in the ear tissue scaffold have been used by our team previously to produce a life-saving, implantable airway device to mitigate severe tracheobronchomalacia.[11,12] Moreover, 3D-printing has been shown to be promising in auricular reconstruction as well.[13,14] The goal of this study was to evaluate the design and initial performance of the auricular scaffold in a pre-clinical animal model study. Our hypothesis was that the two-stage approach would limit the overlying soft tissue strain and thus result in lower rates of soft tissue ulceration, necrosis, and related complications compared to the single-stage reconstruction.[2,15] Both a single- and two-stage version were assessed for feasibility of implantation, aesthetic appearance, histologic outcomes, and complication rates in order to optimize scaffold design.

Materials and methods

Scaffold Design, Manufacturing and Mechanical Testing

This preclinical *in vivo* study was performed in an athymic rodent model with a two-month follow-up. DICOM computed tomography (CT) images of a human auricle were segmented first using automated methods and then manually adjusting the model to create an external anatomic envelope that was filled with orthogonally interconnected spherical pores made for periodically repeated mathematical unit cells as described in prior work.[7,] The unit cell was 2×2×2 mm and the centered spherical pore was 2.4mm in diameter, creating a structure of 59% porosity with completely connected pores. For the two-stage, dove-tail/lock-in-key design, the design envelope was split and three cylinders were created on the second stage insert and three mating slots were created on the first stage insert to assemble the two stage scaffolds. Single- and two-stage versions of these auricular scaffolds were 3D printed by laser sintering poly-L-caprolactone (PCL) (Polysciences, Inc., catalog #25090-B) with a mixture of 4% hydroxyapatite (Plasma Biotal) where the HA serves primarily as a flowing agent for powder spreading during the laser sintering process. PCL was chosen for its bioresorbability, biocompatibility, moldability, thermal stability, and mimicry of extracellular matrix capable of facilitating the proliferation and differentiation of cells *in vitro* and *in vivo*.[15,16] Scaffolds were printed using using an EOS P110 laser sintering system laser sintering under non-sterile conditions but were sterilized by low-temperature ethylene oxide gas sterilization prior to implantation. The laser sintering process was run using the following parameters: laser speed 1800mm/s, laser power 4W, build chamber temperature 54°C, removal chamber temperature 43°C.

Following 3D printing, n=6 single stage scaffolds were tested in helix down compression which was first introduced by Zopf et al.[17] For comparison, completely solid ears with the same geometry as scaffolds (n=6) were also tested in helix down compression. In this test, the whole ear is placed helix down and compressed at a rate of 10mm/min up to 8mm. Geometric stiffness was calculated by a linear regression fit to the load displacement curve using MATLAB (The Mathworks).

Animal Models

NIH guidelines for the care and use of laboratory animals (NIH Publication #85–23 Rev. 1985) have been observed. Male NIH-Foxn1 (strain 316, 7–10 weeks) athymic rats were purchased from Charles River. The animals were housed in Specific Pathogen Free (SPF)/ BSL2 room located in the AAALAC-accredited vivarium at the University of Michigan. All experiments were approved by the Institutional Animal Care & Use Committee (IACUC).

In vivo scaffold implantation

The single-stage construct and the base platform the two-stage reconstructions were each implanted subcutaneously in five rodents. The elevating platform of the two-stage construct was implanted at four weeks. General anesthetic, isofluorane, was administered. A dorsal incision was performed with development of a subcutaneous pocket within which the scaffolds were implanted. Layered skin closure was performed with 4–0 monocryl subcuticular closure, and scaffolds were evaluated weekly to assess the following elements: scaffold dimensions utilizing a standardized measurement system, cross-sectional ulceration area and localization as measured digitally where ulcers were defined as localized areas of tissue damage or necrosis, and signs and symptoms of infection.

After eight weeks, ear constructs were explanted and analyzed radiologically and histologically. For radiology, random samples of scaffold were placed in a 19 mm diameter specimen holder and scanned using a microCT system (μCT100 Scanco Medical, Bassersdorf, Switzerland) with the following settings: voxel size 12 μm, 55 kVp, 109 μA, 0.5 mm AL filter, and integration time 500 ms. Scans were processed using Materialise Mimics to form 3-dimensional (3D) representations. For histology, specimens were fixed with 10% phosphate buffered formalin for 24 hours, and then embedded in paraffin and sectioned using standard histochemical techniques. Serial slide sections were stained with hematoxylin and eosin (H&E) and were used to gauge tissue ingrowth and vascular density. Specifically, samples were taken from three pre-determined locations, and the number and area of blood vessels taken from four random 20x images were evaluated under blinded conditions.

The primary outcomes were differences between the single- and two-stage auricular bioscaffolds in terms of scaffold contraction and distortion, location and cross-sectional ulcer area, and rates of infection as compared by two-tailed t-tests, a test that determines whether a statistically significant difference exists in measures between two populations, where we defined significance as a p value less than than 0.05. The secondary outcomes were number of blood vessels and area, both compared by two-tailed t-test, and localization of strain as measured using nonlinear finite element analysis. The length of time of experimentation was deemed sufficient to measure initial responses to the scaffolds and surgeries and minimize potential duration of discomfort.

Finite Element Analysis

An ear finite element mesh was generated from the original anatomic ear STL file using FEBio PreView2.1. The ear was meshed with 10-node quadratic tetrahedral elements and contained 75,556 elements and 110,126 nodes. The scaffold PCL was modeled as a linear

elastic material with Young's modulus of 200.0 MPa and Poisson's ratio of 0.3. A skin flap was modeled as a box pulled down 10mm over the ear scaffold to simulate surgery implantation and skin coverage. Skin was assumed to undergo large deformation and was modeled as nonlinear elastic material characterized by a 1-term Ogden model – a model used to describe nonlinear stress-strain behavior of complex materials – with a shear modulus of 0.11 MPa and an exponent of 9.[18,19] In addition to the shear modulus μ and the exponent m, the Ogden model incorporates principal stretch ratios λ_i in each Cartesian axis x (i=1), y (i=2) and z (i=3):

$$W = \frac{\mu}{m^2}\left(\lambda_1^m + \lambda_2^m + \lambda_3^m - 3\right)$$

Where W denotes the strain energy function (used as a constitutive model for nonlinear elastic materials), the stretch ratios are the ratio between material lengths in the deformed configuration and the initial (undeformed) configuration. Sliding elastic contact was assumed to occur between the ear scaffold and overlying skin flap during implantation. The analysis was performed using FEBio v 2.80.[20,21]

Results

Single- and two-stage auricular PCL constructs were laser sintered with high fidelity anatomic appearance and interconnected pores (Figure 1). The novel two-staged tissue scaffold facilitated a modular attachment that was successfully engaged with a precise fit in all five surgeries (Figure 2). Single stage auricular scaffolds had a helix down geometric stiffness of 16.52 ± 0.57 Newtons/millimeter (N/mm). This was less stiff than solid PCL scaffolds (87.67 ± 1.68 N/mm) but stiffer than the range of helix down geometric stiffness reported for human ears by Zopf et al. (0.17 to 0.55 N/mm).[17]

The average time required for subcutaneous scaffold implantation was 22.4 ± 4.9 minutes from incision to closure. The overall proportions of the ears were maintained for the entire eight week duration of the *in vivo* analysis and no notable dimensional contracture occurred for either the single- and two-stage constructs. Additionally, by gross comparison with original scaffolds, there was no distortion of auricular subunit landmarks (superior and inferior crus of the antehelix, stem of the antehelix, triangular fossa, scaffoid fossa, conchal bowl, tragal, antetragal, intertragal complex)

After explantation, gross examination of the constructs revealed robust tissue ingrowth and angiogenesis (Figure 3–A). Similarly, on Hematoxylin and Eosin staining, numerous vessels of various sizes were noted (Figure 3–B). MicroCT demonstrated homogenous and complete soft tissue ingrowth and integration visible throughout the PCL pores (Figure 4). There was no significant difference between single- and two-stage constructs when comparing the number of blood vessels (mean 7.0 for single-stage vs 6.7 for two-stage, $p>0.05$) or percent area of blood vessels (mean 2.0% for single-stage vs 2.2% for two-stage, $p>0.05$) per high-powered field.

With the two-stage scaffold, ulcers were seen in all rats with improvements in at least one ulcer seen in 80% of specimens (4/5) by the time of harvest. Of 12 total ulcers, 8 (67%) showed improvement in cross-sectional area, 3 (25%) showed worsening in cross-sectional area, and 1 (8%) showed relative stability in cross-sectional area. With the single-stage scaffold, ulceration occurred in all rodents as well, but improvement in at least one ulcer by the time of harvest seen in 100% of specimens (5/5). Of 12 total ulcers, 8 (67%) showed improvement in cross-sectional area, 3 (25%) showed worsening in cross-sectional area, and 1 (8%) showed relative stability in cross-sectional area (Figure 5). Of note, one of the rats with the two-stage scaffold (Rat 2) was sacrificed at five weeks after implantation due to a surgical dehiscence. Minor superficial ulcers occurred most commonly at the lateral (86% of animals) and superior (29% of animals) helix of the scaffold in either group and demonstrated improvement over time (Figure 6). These findings coincide with locations of maximum skin strains over 18% predicted by the finite element simulation of skin pulled over the PCL ear scaffold (Figure 7).

Discussion

The study demonstrated that consistent patient-specific design and manufacturing methods resulted in unparalleled ear appearance *in vivo*. Our findings indicate that high-fidelity 3D-printed single- and two-stage auricular bioscaffolds can be manufactured and implanted successfully and efficiently. Projection was maintained throughout the eight-week *in vivo* experiment and no contracture was observed. Additionally, histologic and imaging analysis revealed evidence of rapid tissue in-growth and angiogenesis. The length of time chosen for experimentation was chosen because of the nature of our hypothesis, namely in that we were expecting models to have ulcers especially in the single-stage scaffold group. We believed that eight weeks would be sufficient to allow the second surgery of our two-stage scaffold to heal. We also thought that this period of time would minimize potential morbidity to the models and that we could adequately describe acute responses to the scaffold while using these data to design future experiments to assess longer term responses.

Minor complications in the form of ulceration occurred with both the single- and two-stage versions. These were located primarily in the lateral and superior aspects of the helix that corresponded with the finite element strain analysis results of the constructs, and we believe areas of ulceration are at least in part secondary to animal manipulation of the scaffold. Notably, similar ulceration is commonly seen in traditional ear reconstructive techniques as well.[22] A very promising finding was the high rates of improvement in ulceration over time with only a quarter of models demonstrating worsening in ulceration over the course of experimentation. Bolstered by our findings of robust angiogenesis, we suspect the improvement in wound healing is secondary to the angiogenesis and transformation of a bare PCL scaffold to an integrated, vascularized tissue implant. The most significant complication found during this project surgical dehiscence leading to early sacrifice of one of the rats with a 2-stage scaffold. Our animal protocol was written to optimize comfort of the animal. However, we believe that clinically, the dehiscence would have been amenable to a revision surgery. Also of note, use of a temperoparietal fascial flap (TPFF) – wherein tissue overlying the temporal fossa may be dissected out and re-transplanted onto defects of the periorbital, mid-facial, and auricular regions – may likely further mitigate soft tissue

complications, though it is infeasible in this small animal model. Moreover, our teams goal of minimizing soft tissue complications may evolve to a treatment paradigm that ultimately will facilitate implantation without the need for TPFF. Our original hypothesis that gradual introduction of framework and gradated overlying skin strain would decrease overlying soft tissue complications in the two-staged group, was not supported.

Scaffold porous architecture design can significantly affect tissue response to auricular scaffolds through multiple mechanisms. First, pore interconnectivity likely facilitates both vascular and tissue ingrowth. Zopf et al. noted that interconnected periodic pores exhibited increased cartilage growth versus random pore architectures with reduced pore interconnectivity and permeability.[7] Second, pore architecture design modulates overall scaffold geometric stiffness. The spherical pore architecture was 59% porous but reduced overall scaffold geometric stiffness by over 81%. Auricular scaffold stiffness is likely related to skin ulceration and dehiscence complications, with stiffer scaffolds leading to increased complications due to increased skin strains leading to increased skin damage. Thus, using architecture design to reduce scaffold stiffness may mitigate skin complications associated with stiffer scaffolds like dense polyethylene.[5] Solid PCL has elastic modulus close to that reported for high density polyethylene, thus we expect that the helix down stiffness of solid PCL will be close to that reported for high density polyethylene auricular reconstruction implants.[5] Thus, porous architecture design may improve auricular reconstruction outcomes by 1) reducing skin complications by reduced scaffold stiffness and thus skin strains and 2) by allowing increased tissue and vascular ingrowth that will enhance reconstruction and accelerate healing of skin ulceration.

Limitations to our work include relatively basic histological analysis. H&E was used to assess for vascularization. Quantification of angiogenesis has inherent challenges based off of how the histology captures the blood vessels and the lack of specificity of H&E to stain vessels. As such, looking forward, we would look to more objectively identify and quantify vessel ingrowth.

The relative ease of implantation and anatomic accuracy makes 3D-printed bioscaffolds an appealing alternative treatment for auricular reconstruction. Reconstruction using autologous rib cartilage grafts involves multiple operative stages with an average operation time of 4 hours and entails extreme technical difficulty.[2,23] In contrast, the average operation time for the scaffold implantation time was under 25 minutes and the steps involved were much simpler. Other benefits of the auricular scaffold include the absence of a required donor site. The resection of multiple ribs required for rib cartilage grafting is associated with numerous complications which can range from severe post-operative pain and rehabilitation requirements to life-threatening infection and pneumothorax.[3] The resulting anatomic appearance of the bioscaffold was extremely realistic and met or exceeded even the best outcomes of rib cartilage grafting. The absence of contraction or distortion over the course of the experiment suggests that the construct shape is durable and will serve as the scaffold for an anatomically intact ear.

The evidence of robust tissue ingrowth and angiogenesis on gross exam and on histology suggests that the scaffold could ultimately support the growth of cartilaginous tissue

formation. Our team's prior studies have supported this idea using seeded scaffolds.[24] The interconnected pore design of the auricular scaffold matrix provides sufficient permeability to aid in supplying cellular growth and nutrition.[25] Future studies will assess the ability to populate these constructs by imparting chondrogenicity to precursor cells. Moreover, additional work is necessary to assess the potential to cellularize the scaffold with the ultimate goal of gradual replacement with a native cartilage matrix, and our group is currently engaged in longer term studies to assess the impact on clinical outcomes in cellularized vs. uncellularized scaffolds.

The results indicate that ulceration peaks approximately two weeks after implantation of the elevating part of the construct, which is the second stage of the two-stage scaffold, but subsequently decreases throughout the remainder of the experiment. The locations of ulceration parallel the areas of high strain demonstrated on finite element analysis. In our next steps, we intend to introduce cells to the scaffolds and assess the impact of this cellularization on wound formation. Populating these constructs with chondrocytes into these same high-strain areas may potentially improve soft tissue coverage and clinical outcomes and decrease ulceration rate.

Conclusion

These preliminary animal model studies demonstrate that the single- and two-staged auricular scaffold designs provide a strong potential alternative to existing auricular reconstruction techniques. The scaffolds demonstrated unparalleled ease of implantation, superb appearance, vascularization, and equivalent rates of superficial wound complications in an *in vivo* athymic rodent model, suggesting that this method could improve upon the limitations of the current standard of care.

Acknowledgements

We would like to acknowledge the Animal Care and Use Program at the University of Michigan for their assistance in animal care and the ASPO Research Career Development Grant for their funding of this work.

Disclosures

AC, SC, ZN, and IL have no conflicts of interest to disclose. JB was funded during this research by the T32 DC005356 NIH pre-doctoral research grant. BC was funded through the MICHR TL1 Grant Number TL1TR002242 during the 2018–2019 school year while the project was being completed but was not specifically funded for this project. SH is a co-founder and shareholder in Tissue Regeneration Systems Inc. SH and DZ are co-inventors on a patent entitled "Ear tissue implant for auricular tissue reconstruction." DZ obtained funding through the ASPO Career Research Development Grant and is a founder in the University of Michigan affiliated start-up MakeMedical, but the company was formed after this experimentation occurred and research was not funded or supported in any way by this entity.

References

1. Pruzinsky T Social and psychological effects of major craniofacial deformity. Cleft Palate Craniofac J 1992;29:578–584. [PubMed: 1450200]
2. Nagata A A new method of total reconstruction of the auricle for microtia. Plast and Reconstr Surg 1993;92:187–201. [PubMed: 8337267]
3. Fling PW, Haughey BH, Lund VJ, et al. Cummings Otolaryngology. Philadelphia: Elsevier; 2015. 3624 p.

4. Thomson HG, Kim TY, Ein SH. Residual problems in chest donor sites after microtia reconstruction: a long-term study. Plast Reconstr Surg 1995;95:961–968. [PubMed: 7732143]
5. Constantine KK, Gilmore J, Lee K, Leach J Jr Comparison of microtia reconstruction outcomes using rib cartilage vs porous polyethylene implant. JAMA Facial Plast Surg 2014;16:240–244. [PubMed: 24763669]
6. Kamil SH, Vacanti MP, Aminuddin BS, Jackson MJ, Vacanti CA, Eavey RD. Tissue engineering of a human sized and shaped auricle using a mold. The Laryngoscope 2004;114:867–870. [PubMed: 15126746]
7. Zopf DA, Mitsak AG, Flanagan CL, Wheeler M, Green GE, Hollister SJ. Computer aided-designed, 3-dimensionally printed porous tissue bioscaffolds for craniofacial soft tissue reconstruction. Otolaryngol - Head Neck Surg 2015;152:57–62. [PubMed: 25281749]
8. Jeong CG, Zhang H, Hollister SJ. Three-dimensional poly(1,8-octanediol-co-citrate) scaffold pore shape and permeability effects on sub-cutaneous in vivo chondrogenesis using primary chondrocytes. Acta Biomater 2011;7:505–514. [PubMed: 20807597]
9. Hollister SJ, Lin CY, Saito E et al. Engineering craniofacial scaffolds, Orthod Craniofacial Res 2005;8:162–173.
10. Hollister SJ. Porous scaffold design for tissue engineering. Nature Materials 2006;5:590.
11. Zopf DA, Hollister SJ, Nelson ME, Ohye RG, Green GE. Bioresorbable airway splint created with three-dimensional printer. N Engl J Med 2013;368:2043–45. [PubMed: 23697530]
12. Les AS, Ohye RG, Filbrun AG et al. 3D-printed, externally implanted, bioresorbable airway splints for severe tracheabronchomalacia. Laryngoscope 2019:129:1763–1771. [PubMed: 30794335]
13. Lee JS, Kim BS, Seo D et al. Three-dimensional cell printing of large-volume tissues: application to ear regeneration. Tissue Eng Part C Methods 2017:23(3):136–145. [PubMed: 28093047]
14. Bichara DA, O'Sullivan NA, Pomerantseva I, et al. The tissue-engineered auricle: past, present, and future. Tissue Eng. Part B Rev 2011;18(1):51–61. [PubMed: 21827281]
15. Bauer BS. Reconstruction of Microtia. Plast Reconstr Surg 2009;124:142e–26c.
16. Siddiqui N, Asawa S, Birru B, Baadhe R, Rao S. PCL-based composite scaffold matrices for tissue engineering applications. Molecular Biotech 2018;60:506–532.
17. Zopf DA, Flanagan CL, Nasser HB, Mitsak AG, Huq FS, Rajendran V, Green GE, Hollister SJ. Biomechanical evaluation of human and porcine auricular cartilage. Laryngoscope. 2015;125(8):E262–8. Epub 2015/04/22. doi: 10.1002/lary.25040. [PubMed: 25891012]
18. Shergold OA, Fleck NA. Experimental investigation into the deep penetration of soft solids by sharp and blunt punches, with application to the piercing of skin. J Biomech Eng 2005;127:838–848. [PubMed: 16248314]
19. Shergold OA, Fleck NA. Mechanisms of deep penetration of soft solids with application to the injection and wounding of skin. Proc. R. Soc. Lond. A 2004;460:3037–358.
20. Maas SA, Ateshian GA, Weiss JA. FEBio: History and Advances. Ann Rev Biomed Eng 2017;19:279–299. [PubMed: 28633565]
21. Maas SA, Ellis BJ, Ateshian GA, Weiss JA. FEBio: finite elements for biomechanics. J Biomech Eng. 2012;134:011005. [PubMed: 22482660]
22. Romo T, Baratelli R, Raunig H. Avoiding complications of microtia and otoplasty. Facial Plast Surg. 2012;28:333–339. [PubMed: 22723235]
23. Han SE, Lim SY, Pyon JK, Bang SI, Mun GH, Oh KS. Aesthetic auricular reconstruction with autologous rib cartilage grafts in adult microtia patients. J Plast Reconstr Aesthet Surg 2015;68:1085–1094. [PubMed: 26026221]
24. Zopf DA, Flanagan CL, Mitsak AG, Brennan JR, Hollister SJ. Pore architecture effects on chondrogenic potential of patient-specific 3-dimensionally printed porous tissue bioscaffolds for auricular tissue engineering. Int J Pediatr Otorhinolaryngol 2018;114:170–174. [PubMed: 30262359]
25. Mitsak AG, Kemppainen JM, Harris M, Hollister SJ. Effect of polycaprolactone permeability on bone regeneration in vivo. Tissue Eng 2011;17:1831–1839.

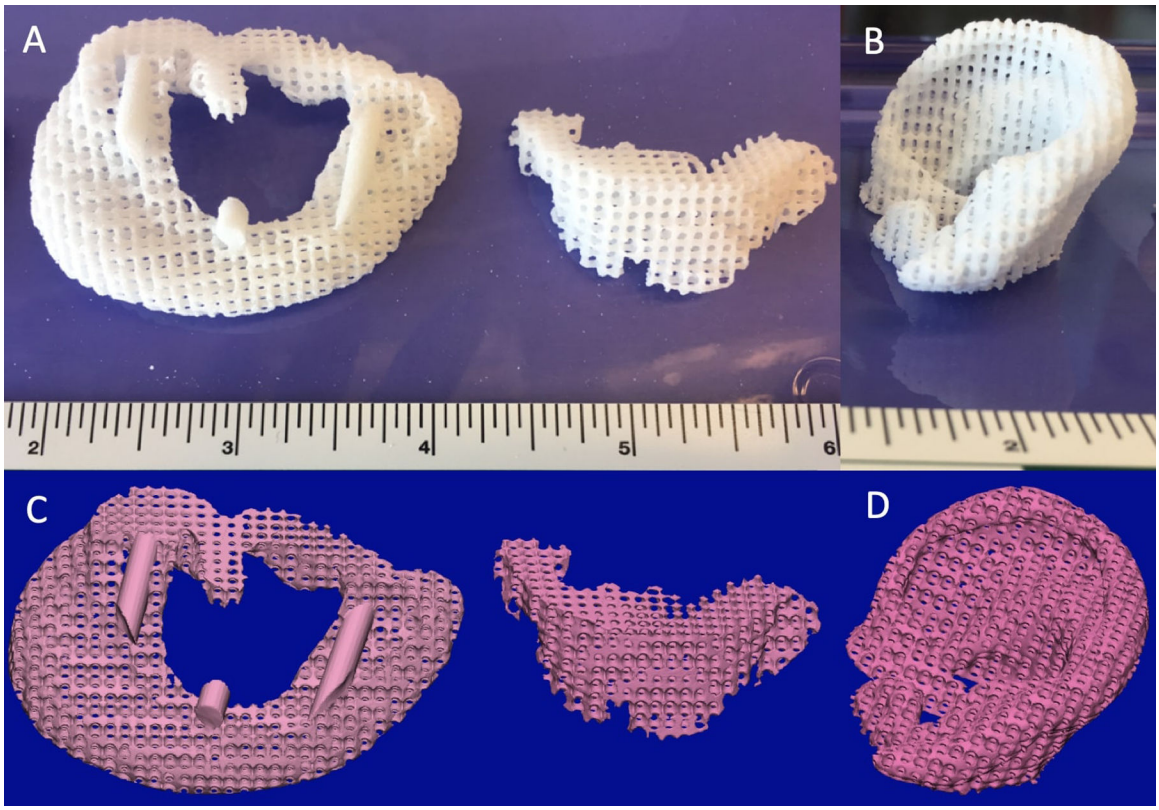

Figure 1:

3D printed (laser sintered) auricular cartilage scaffolds. A – Laser sintered PCL Two-stage, lock-in-key design. B – Laser sintered PCL Single-stage design. C – Image-designed STL file for two-stage, lock-in-key design. D – Image-designed STL file for single-stage design.

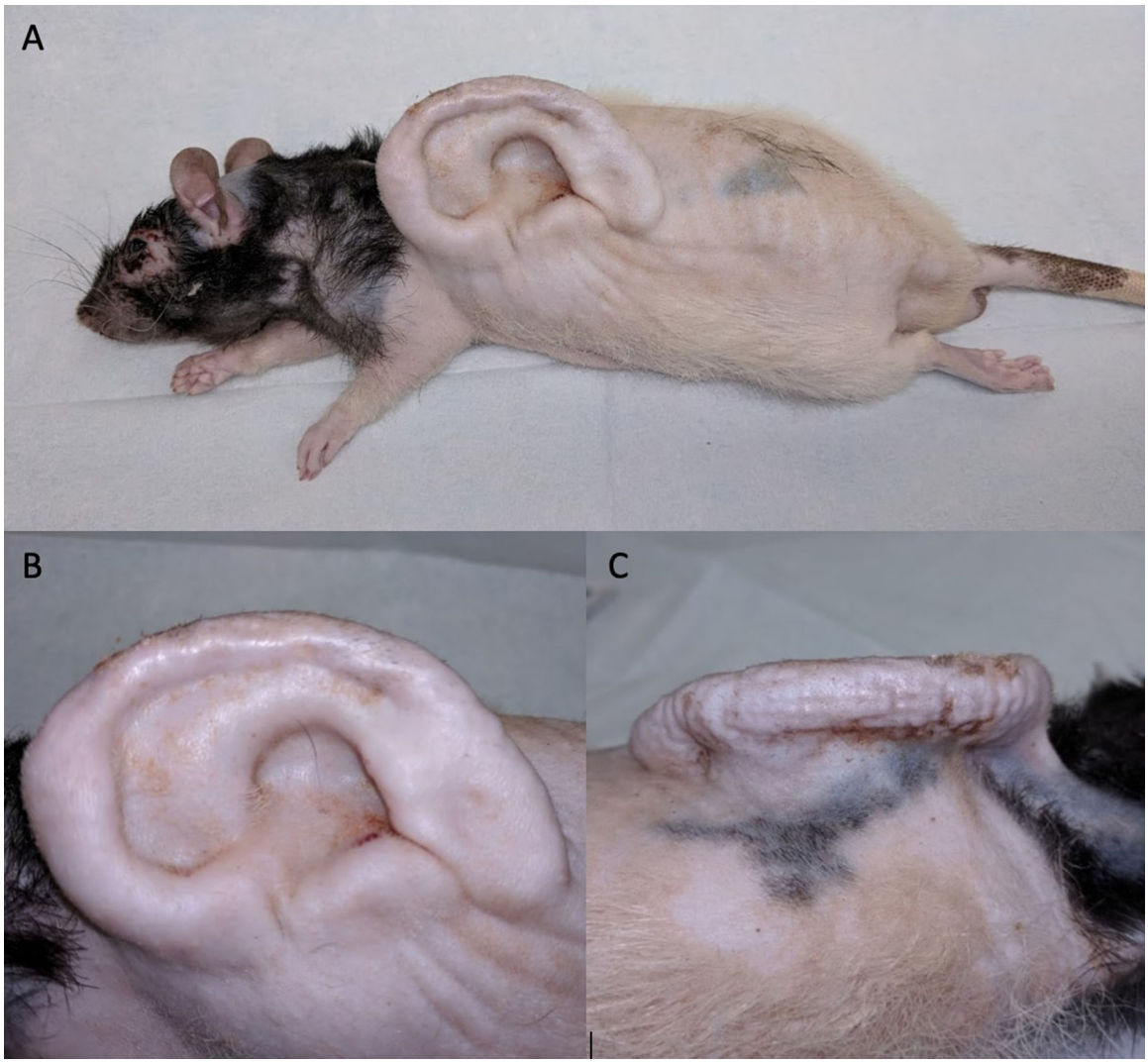

Figure 2:
Representative views of an ear scaffold implanted on the dorsum of the rat. A and B – Lateral view demonstrating anatomic integrity of ear scaffold. C – View demonstrating ear scaffold projection.

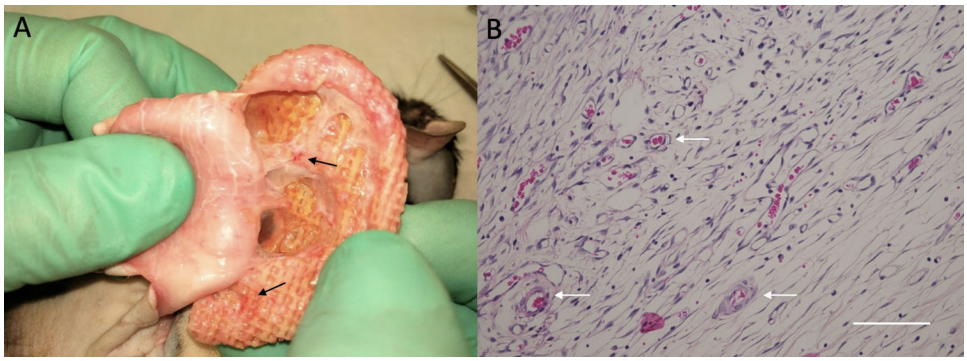

Figure 3:
Images showing evidence of angiogenesis upon harvesting the scaffolds at 8 weeks. A – View demonstrating evidence of angiogenesis on gross examination. B – Representative microscopic image demonstrating vasculature ingrowth on Hematoxylin and Eosin staining, where the scale bar represents 100 microns. Vascularization is noted by the arrows.

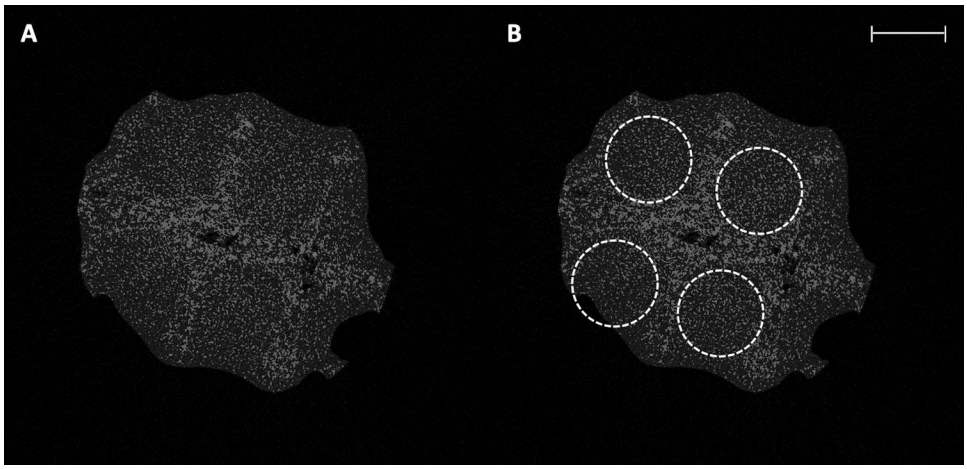

Figure 4:
A – μCT image of scaffold slice demonstrating homogenous tissue ingrowth throughout scaffold pores. B – The same μCT image with scaffold pores outlined. Scale bar represents 2 mm.

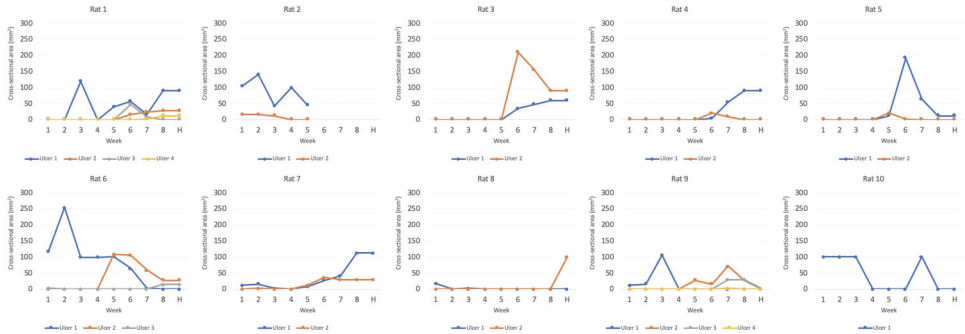

Figure 5:

Cross-sectional ulcer size for two-stage (rats 1–5) and single-stage scaffolds (rats 6–10). Y-axis represents cross-sectional area in mm^2 and X-axis represents week after implantation, where H is the date of harvest.

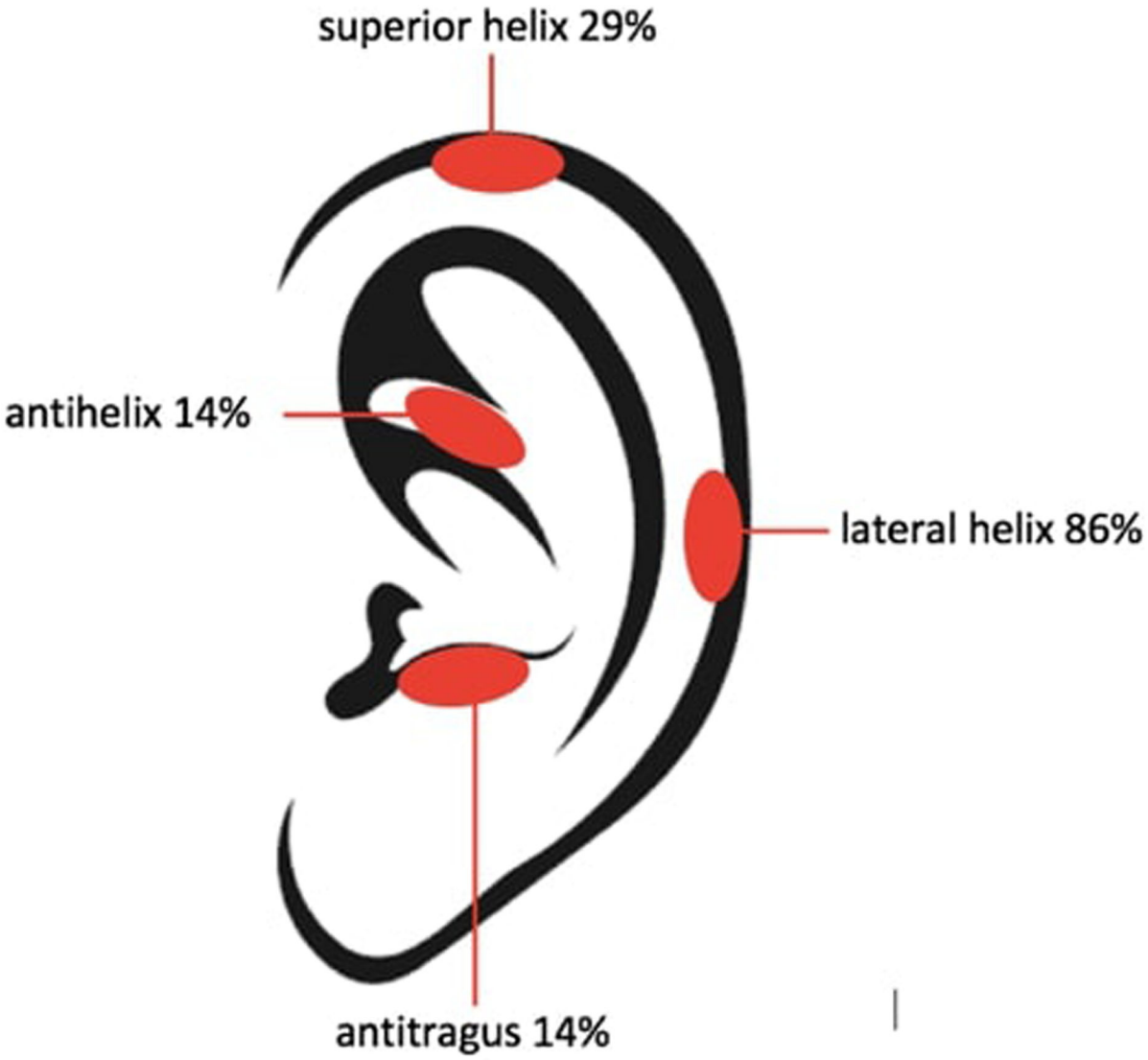

Figure 6:

A regional map of ulcer development reveals areas more prone to skin breakdown by establishing the percent of ulcers that developed in the indicated area. Percentage numbers refer to the percent of animals exhibiting ulcerations at the indicated area.

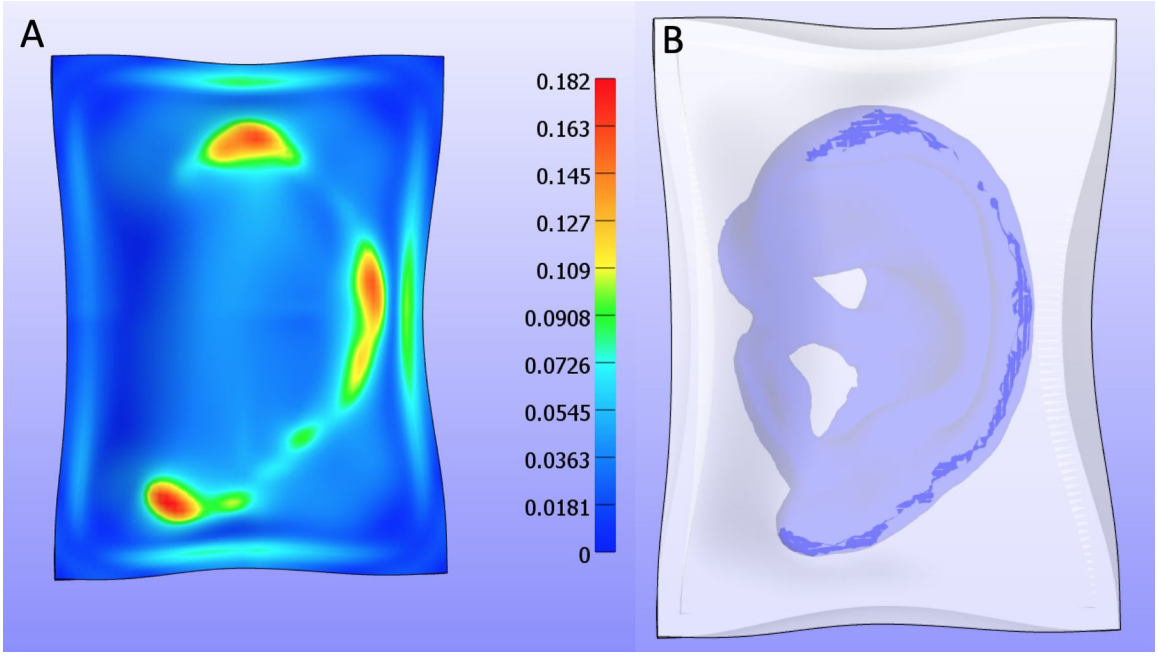

Figure 7:

First Principal Lagrange Finite Strain (tension) after pulling skin over PCL ear construct. A – Maximum strains of 18% are seen in lateral helix and superior helix areas which coincide with most frequent areas of ulceration (86%) and (29%) respectively. B – Location of high contact areas (dark blue) underneath skin model that has been made transparent.